applied sciences

MDPI

Article

A Switching Observer for State-of-Charge Estimation of Reconfigurable Supercapacitors

Heng Li †, Zitao Zhou † and Chao Hu *

School of Electronic Information, Central South University, Changsha 410083, China; liheng@csu.edu.cn (H.L.); 8208211514@csu.edu.cn (Z.Z.)

* Correspondence: huchao@csu.edu.cn

† These authors contributed equally to this work.

Abstract: While State-of-Charge (SOC) estimation for supercapacitors has been extensively studied, most research focuses on single units. However, the recent introduction of reconfigurable circuits significantly alters system dynamics, rendering existing SOC estimation techniques inadequate. This paper addresses this challenge by employing a switching systems approach to estimate the SOC of supercapacitors with reconfigurable circuits. We first establish an RC model for the supercapacitor integrated with the reconfigurable circuit and thoroughly analyze the state continuity and observability of the resulting switched system. Subsequently, we propose a switching observer and evaluate its convergence properties by comparing its performance against other observer techniques. Experimental validation on a hardware platform demonstrates the superiority of our proposed observer for accurate SOC estimation in this context.

Keywords: switching observer; linear switching system; reconfigurable circuits; state of charge; supercapacitors

Citation: Li, H.; Zhou, Z.; Hu, C. A Switching Observer for State-of-Charge Estimation of Reconfigurable Supercapacitors. *Appl. Sci.* **2024**, *14*, 8005. https://doi.org/10.3390/app14178005

Academic Editors: Paulo Rocha and Bahram Gharabaghi

Received: 1 August 2024
Revised: 2 September 2024
Accepted: 5 September 2024
Published: 7 September 2024

1. Introduction

Supercapacitors have emerged as promising energy storage devices due to their exceptional performance, finding applications in electric vehicles, renewable energy systems, and modern power grids [1], and research on it continues to be updated [2]. As a commonly used onboard power source for electric vehicles, the State of Charge (SOC) of supercapacitors is a key parameter that reflects the current charge storage level. Accurate SOC estimation is fundamental to energy control and management, ensuring the safe and reliable operation of the onboard power system, which is crucial for maintaining its operational efficiency and longevity [3]. At times we need to ensure that the SOC operates within a certain range to guarantee the system's proper functioning [4].

Due to the importance of the SOC in supercapacitors, many methods for estimating the SOC have already been proposed [5]. While traditional Coulomb counting is straightforward, its accuracy diminishes under dynamic conditions due to the gradual accumulation of errors over time. Data-driven approaches for estimating battery SOC [6], like deep feedforward neural networks (DNNs) [7], Elman neural networks [8], and long short-term memory recurrent neural networks (LSTM RNNs) [9] provide greater accuracy but come with higher computational demands and a reliance on data quality. These methods often necessitate the frequent retraining of the model. In contrast, model-based techniques such as Luenberger observers, sliding-mode observers [10], Kalman Filters, and nonlinear observers [11] strike a balance between computational efficiency and accuracy. The Kalman Filter is one of the most widely used methods, and different types of Kalman Filters have already been applied to SOC estimation, including the Extended Kalman Filter (EKF) [12,13], Adaptive Kalman Filter (AKF) [14], and Unscented Kalman Filter (UKF) [15,16].

However, most existing research primarily focuses on individual supercapacitor cells, utilizing cell current as input and cell voltage as output for observer design. In practical

applications, supercapacitors are rarely used in isolation and are often integrated with balancing circuits [17–19]. Reconfigurable circuits have recently emerged as a promising solution to address balancing challenges in battery and supercapacitor applications [20]. These circuits enable dynamic reconfiguration to adjust voltage and current levels, optimize energy conversion efficiency, and isolate faulty cells, ultimately extending the lifespan of the energy storage system. However, the switching actions inherent in reconfigurable circuits introduce abrupt changes in the system model, rendering traditional observers ineffective.

This paper proposes a novel SOC estimation method for supercapacitors integrated with reconfigurable circuits based on a switched systems approach. We develop a linear switched system model to capture the dynamic behavior of the system. A corresponding observer is designed, explicitly considering the impact of switching events on system dynamics. Experimental results validate the effectiveness of the proposed method.

2. Modeling and Motivation

2.1. System Modeling

This section details the development of a suitable model for supercapacitors integrated with reconfigurable circuits.

2.1.1. Supercapacitor Representation

Figure 1 illustrates the adopted supercapacitor model, employing a series connection of RC circuits. This representation is widely used due to its balance of accuracy and simplicity.

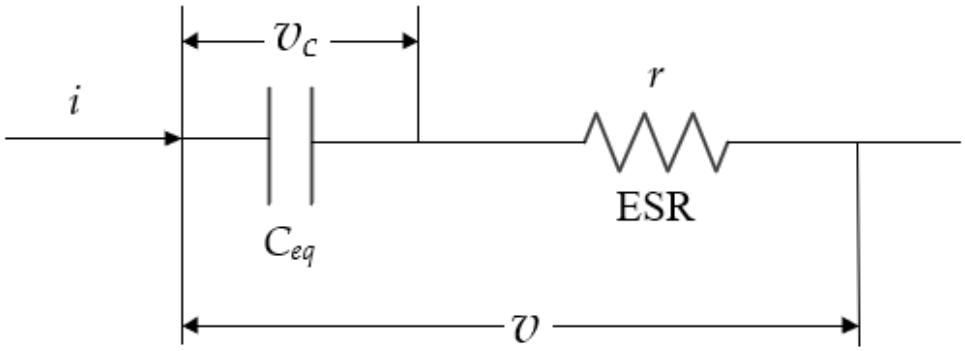

Figure 1. The equivalent RC circuit of the supercapacitor.

While often small in magnitude, the impact of Equivalent Series Resistance (ESR) can contribute to power dissipation within the system. In reality, ESR is a parameter that is almost impossible to measure accurately and can vary over time. We will discuss the impact of this variation in the observer design and experiment sections. State of Charge (SOC) serves as a crucial metric for supercapacitors, reflecting the available charge relative to its capacity. SOC is commonly defined as

$$\text{SOC} = \frac{Q_{remain}(t)}{Q_{rated}} \times 100\% \tag{1}$$

where $Q_{remain}(t)$ represents the remaining charge at time instant t, and Q_{rated} denotes the rated charge, which remains constant.

It is important to note that in certain cases, Q_{rated} might be replaced with the maximum available capacity, which tends to be lower than the rated capacity due to the impact of continuous charge–discharge cycles.

Let v_{rated} represent the rated maximum voltage, v the terminal voltage of the supercapacitor cell, and $v_c(t)$ the voltage across the equivalent capacitor of the cell. Based on the fundamental characteristics of a capacitor, we have

$$Q_{remain} = C_{eq} v_c(t) \tag{2}$$

$$Q_{rated} = C_{eq} v_{rated} \tag{3}$$

where C_{eq} represents the equivalent capacitance of the supercapacitor.

Combining Equations (1)–(3), we can derive the following relationship:

$$\text{SOC} = \frac{v_c(t)}{v_{rated}} \tag{4}$$

Considering the influence of ESR, the voltage across the equivalent capacitor can be expressed as

$$v_c = v - ir \tag{5}$$

where i represents the charging current flowing through the cell, and r denotes the ESR of the cell. The voltage dynamics across the equivalent capacitor C_{eq} can be described by

$$\dot{v}_c = \frac{i}{C_{eq}} \tag{6}$$

It is crucial to observe that a higher charging current i leads to a faster rate of change in the voltage v_c.

Differentiating both sides of Equation (4) with respect to time, we obtain

$$\dot{SOC} = \frac{i}{C_{eq} v_{rated}} \tag{7}$$

2.1.2. Reconfigurable Circuit Modeling

Let us begin by examining the reconfigurable circuit illustrated in Figure 2. This circuit features two switches, s controlling the capacitor branch and $\bar{s}$ governing the bypass path. These switches operate in a complementary fashion, ensuring that only one path is active at any given time. When s is ON ($s = 1$), the supercapacitor is connected to the main circuit, allowing for charging or discharging. Conversely, when $\bar{s}$ is ON ($\bar{s} = 1$), the supercapacitor is bypassed, effectively isolating it from the circuit and preventing any current flow.

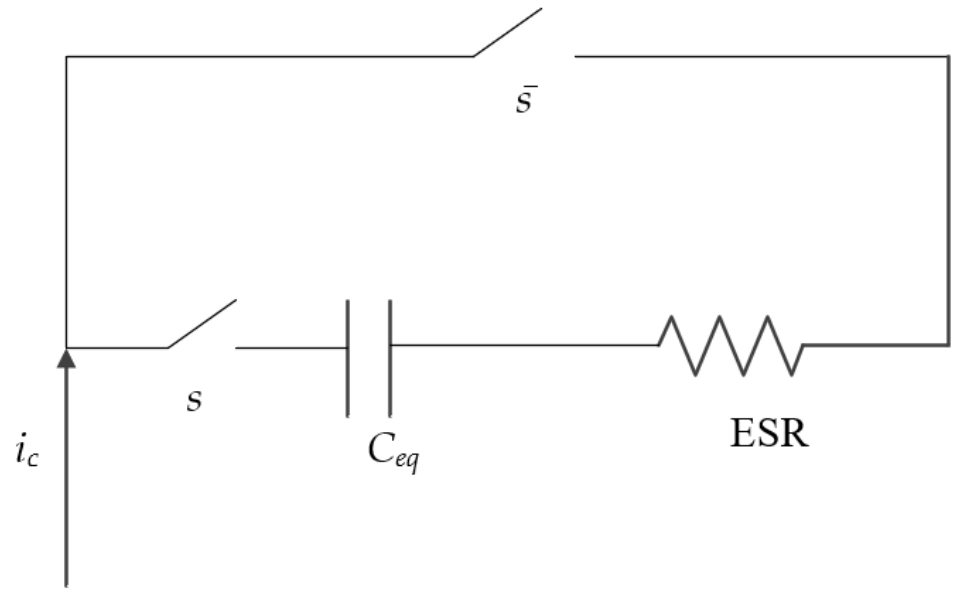

Figure 2. The reconfigurable circuit considering ESR.

To develop a comprehensive model for cell balancing, we need to integrate the mathematical representations of both the supercapacitor and the reconfigurable circuit. This integrated model will provide a framework for analyzing and controlling the system's behavior.

By combining Equations (5) and (7), which describe the supercapacitor's dynamics, with Equations (4) and (6), which capture the circuit configuration, we arrive at the following state-space representation for the supercapacitor within the reconfigurable circuit:

$$\begin{cases} \dot{SOC} = \frac{s}{C_{eq} v_{rated}} i \\ v = v_{rated} SOC + sri \end{cases} \tag{8}$$

In this representation, i represents the input current, v represents the output voltage, and SOC serves as the state variable, reflecting the supercapacitor's charge level. This model reveals that the system exhibits switching behavior, transitioning between two distinct linear subsystems depending on the state of the switches.

To further clarify the system's dynamics, we can compare Equation (8) with the general form of a state-space representation:

$$\begin{cases} \dot{x} = A_\sigma x + B_\sigma u \\ y = C_\sigma x + D_\sigma u \end{cases} \tag{9}$$

In this general form, x represents the state vector, u represents the input vector, and y represents the output vector. The matrices A_σ, B_σ, C_σ, and D_σ define the system's behavior in each subsystem, with the subscript σ indicating the active subsystem.

By mapping the variables in our specific model ($x = SOC$, $u = i$, $y = v$) to the general form, we can readily extract the system parameters for each subsystem:

$$A_1 = 0, B_1 = 0, C_1 = v_{rated}, D_1 = 0 \tag{10}$$

$$A_2 = 0, B_2 = \frac{1}{C_{eq} v_{rated}}, C_2 = v_{rated}, D_2 = r \tag{11}$$

Here, $\sigma = s + 1$ serves as a switching signal, determining which set of parameters is active at any given time. When $\sigma = 1$ ($s = 0$), the supercapacitor is bypassed, and the system's behavior is governed by the parameters in Equation (10). Conversely, when $\sigma = 2$ ($s = 1$), the supercapacitor is connected, and the system's behavior is dictated by the parameters in Equation (11).

2.2. Motivation

2.2.1. Challenges in SOC Estimation for Reconfigurable Circuits

Accurately estimating the State-of-Charge (SOC) of supercapacitors in reconfigurable circuits presents unique challenges. Let us consider a scenario where an external charging current, denoted as i_c, supplies the circuit. This current can be constant or time-varying, and for a more general analysis, we assume it changes over time. The actual current flowing through the supercapacitor, representing the system input, is denoted by u.

Figure 3 illustrates the impact of reconfigurable circuitry on SOC estimation. The figure depicts a 20-second charging sequence with a time-varying charging current. To highlight the effects of circuit switching, we intentionally open switch s (turning it OFF) during two intervals: from 0 to 5 s and from 10 to 15 s.

Note that when the switch is turned off, meaning $s = 0$, the charging current through the supercapacitor drops to zero, as shown in the figure. This abrupt change in current poses a significant problem for conventional SOC estimation techniques that rely solely on the external charging current (i_c) and a single supercapacitor model. In such cases, the input current error approaches 100%, rendering the SOC estimation inaccurate and unreliable.

Furthermore, Figure 3 demonstrates that the supercapacitor voltage can be maintained at a constant level when the switch is OFF. This ability to isolate and hold the supercapacitor's voltage highlights the potential benefits of reconfigurable circuits in energy management and power control applications.

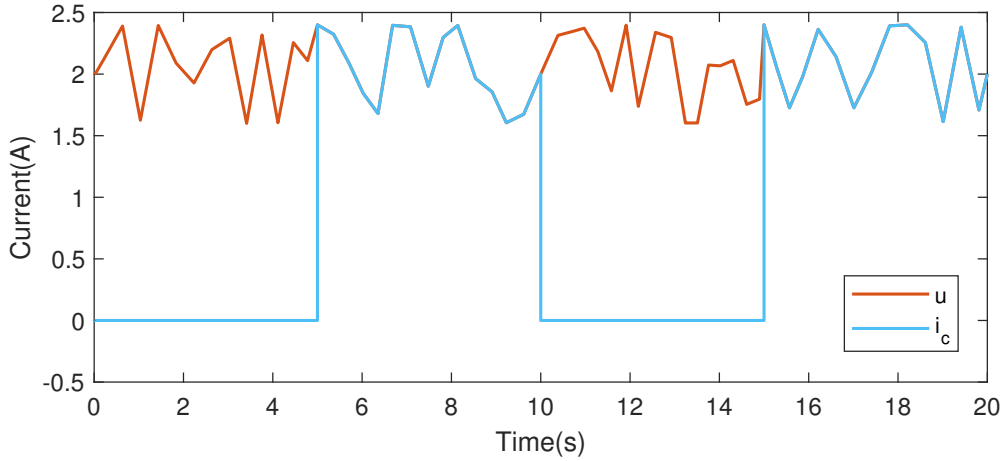

Figure 3. Supercapacitors charging during circuit switching.

2.2.2. Limitations of Open-Loop SOC Estimation

While Equation (8) provides a direct relationship between SOC, SȮC, voltage, and current, it raises a crucial question: can we rely solely on this equation for accurate SOC estimation in a reconfigurable circuit?

By deforming the first line of Equation (8), we can easily obtain the open-loop calculation equation for SOC:

$$\mathrm{SOC(t)} = \mathrm{SOC(0)} + \Delta\mathrm{SOC} = \mathrm{SOC(0)} + \int_0^t \frac{s}{C_{eq} v_{rated}} i(t)dt \tag{12}$$

In the equation, SOC(0) represents the initial SOC.

To investigate this, let us analyze a charging scenario where a supercapacitor with a rated voltage (v_{rated}) of 2.7 V, an internal resistance (r) of 2.2 mΩ, and a capacitance of 310 F (C_{eq}) is charged with a constant current of 2 A (i). Once fully charged, switch s is toggled to open the supercapacitor branch.

Clearly, when evaluating the SOC estimation using the open-loop method, we must consider not only the cases where the parameters are precise but also where there are errors in the parameters. Here, we simulate the real-world scenario where supercapacitor parameters may have errors by modifying the capacitance value (C_{eq}) in Equation (12). As for the true SOC, we can directly adjust Equation (8) to obtain Equation (13), using the actual parameters of the supercapacitor for calculation:

$$\mathrm{SOC} = \frac{v - sri}{v_{rated}} \tag{13}$$

Figure 4 shows the SOC estimation results obtained using the open-loop method described by Equation (12) in the simulation experiment. To simulate real-world measurement uncertainties, we considered two scenarios: one where the capacitance (C_{eq}) in Equation (12) matches the true value and another where there is a 10% deviation from the true value. Although the open-loop estimation performs well when the parameters are accurate, it fails to converge to the true SOC value when there are parameter errors, as seen in Figure 4a and Table 1. This divergence highlights a significant drawback of the open-loop approach: its susceptibility to measurement errors, which are inevitable in practical applications. Therefore, a more robust approach is needed to address this limitation. Additionally, to further confirm the limitations of the open-loop estimation, we will also use this method in subsequent hardware experiments.

Table 1. Open-loop estimation performance under capacitance changes.

	Initial SOC (%)	Final SOC (%)	Charging Stop Time (s)
True Value	30.12	100.03	293.164
Open-loop Observer	30.12	93.62	293.164

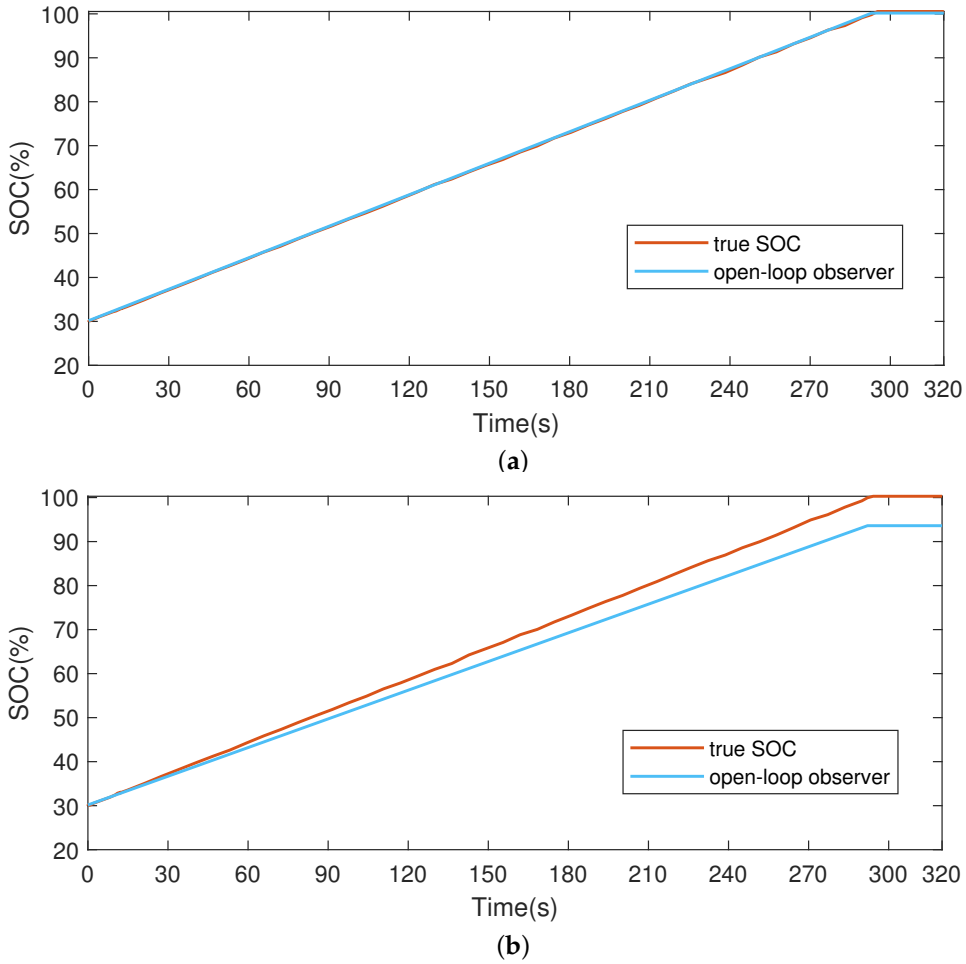

Figure 4. Comparison of SOC estimation performance during dynamic charging with capacitance variations. (**a**) SOC estimation with 10% capacitance variations. (**b**) SOC estimation with 10% capacitance variations.

3. Observer Design for Switching Systems

Due to the different state-space equation parameters of the system at different operating points, switching observers are considered. In this section, we will propose a usable switching observer based on the proof of properties.

3.1. System Properties

Before delving into observer design, it is essential to understand the fundamental properties of our switching system, which are crucial for observer construction. These properties encompass continuity, state differentiability, and the controllability and observability of each subsystem.

Lemma 1. *Consider the switched system described by the state-space Equation (8), where the input current i is piecewise continuous. Then, the system's state (SOC) is continuous due to its differentiability.*

Proof. To prove the continuity of the state, we need to demonstrate its differentiability. This involves establishing the existence and uniqueness of solutions for the state-space Equation (8) and showing that the equation itself is continuous. □

From Equation (8), we can derive the following differential equation:

$$\dot{\mathrm{SOC}} = f(t, \mathrm{SOC}, \lambda) \tag{14}$$

Here, λ represents the system parameters, including r, C, R, and s, while $i(t)$ is a piecewise continuous function of time.

Let us define $T = \{t_l\}_{l=1}^{\infty}$ as the sequence of switching instants. We assume that $i(t)$ remains continuous within each time interval (t_l, t_{l+1}) and that the system is Zeno-free, meaning that it does not exhibit infinitely fast switching. Consequently, within each interval (t_l, t_{l+1}), the impact of switching remains bounded.

Now, we invoke a mathematical principle: if a function remains bounded within a finite time interval, both its left-hand and right-hand limits must exist at every point within that interval.

Proof of the Principle. The principle clearly holds for points where the function is continuous. Let us focus on discontinuities. □

Consider approaching a point t from the left, denoted as $t \to t_{l-}$. Due to the function's boundedness in the interval $[t_0, t_l]$, any sequence t_n approaching t_l from the left ($t_n < t_l$ and $t_n \to t_l$) will result in a bounded sequence $g(t_n)$. This implies the existence of a finite limit L_l such that $\lim_{t \to t_{l-}} g(t) = L_l$.

Similarly, approaching t from the right ($t \to t_{l+}$) leads to the existence of a finite right-hand limit L_r such that $\lim_{t \to t_{l+}} g(t) = L_r$.

Therefore, at any jump point $t = t_l$, both the left-hand and right-hand limits of $g(t)$ exist. This allows for discontinuities of the first kind, where the function takes a finite jump.

Consequently, we can conclude that $f(t, SOC, \lambda)$ is piecewise continuous in t, as discontinuities of the first kind do not disrupt the function's continuity at other points.

Next, let us examine the Lipschitz constant of f with respect to SOC:

$$\frac{\left| f(t, \mathrm{SOC}_x, \lambda) - f(t, \mathrm{SOC}_y, \lambda) \right|}{\left| \mathrm{SOC}_x - SOC_y \right|} \leq L \tag{15}$$

Since f is independent of SOC, the left-hand side of the inequality is always zero. Therefore, the inequality holds true for any value of L, including $L = 0$, regardless of whether $s = 0$ or $s = 1$.

Lemma 2. *The switching system represented by Equation (8) maintains observability regardless of the switch state.*

Proof. To assess the observability of the system, let us examine the controllability and observability matrices derived from Equations (10) and (11):

$$\mathrm{C}_1 = 0, \mathrm{C}_2 = \frac{1}{C_{eq} v_{rated}} \tag{16}$$

$$\mathrm{O}_1 = v_{rated}, \mathrm{O}_2 = v_{rated} \tag{17}$$

These matrices reveal the following ranks: $rank(C_1) = 0$, $rank(C_2) = 1$, $rank(O_1) = 1$, and $rank(O_2) = 1$. □

When the capacitor is short-circuited ($s = 0$), the system becomes uncontrollable, as indicated by $rank(C_1) = 0$. However, crucially, the system remains observable in both switch states, evidenced by the full rank of the observability matrices ($rank(O_1) = rank(O_2) = 1$).

Therefore, even though controllability is lost when the capacitor is short-circuited, the system's observability persists, allowing us to estimate the state (SOC) based on the available measurements.

3.2. Observer Design

Having established the system's properties, we can now proceed to design a switching observer tailored to our specific system dynamics. Equation (8) provides the foundation for constructing this observer.

The proposed switching observer takes the following form:

$$\begin{cases} \dot{\hat{\text{SOC}}} = A_\sigma \hat{\text{SOC}} + B_\sigma i + L_\sigma (v - \hat{v}) \\ \hat{v} = C_\sigma \hat{\text{SOC}} + D_\sigma i \end{cases} \tag{18}$$

In this observer structure, L_σ represents the observer gain, a crucial design parameter that needs careful selection to ensure the estimated state, and $\hat{\text{SOC}}$ converges asymptotically to the true state, SOC.

To analyze the observer's convergence, we can combine Equation (8) with Equation (18) to obtain the error dynamics:

$$\dot{e} = \bar{A}_\sigma e \tag{19}$$

Here, $e = \hat{\text{SOC}} - \text{SOC}$ represents the estimation error. Our goal is to ensure the asymptotic stability of this error system. The matrix $\bar{A}_\sigma$ governing the error dynamics is given by

$$\bar{A}_\sigma = A_\sigma - L_\sigma C_\sigma \tag{20}$$

By carefully choosing the observer gain L_σ, we can manipulate the eigenvalues of $\bar{A}_\sigma$ to ensure that the error dynamics converge to zero, implying that our estimated SOC will approach the true SOC over time.

Next, let us discuss the errors introduced by parameter variations. When the supercapacitor is not charging, both A_σ and B_σ in the equation are 0, so the observed SOC remains constant. However, when the switch is switched and the supercapacitor starts charging, parameter variations will have an impact. Take ESR as an example, which is a parameter often subject to errors.

When the ESR changes, that is, when D_σ changes, and assuming the change value is ΔD_σ, a new error term will be introduced:

$$e_y = y - \hat{y} = (D_\sigma + \Delta D_\sigma - D_\sigma)u = \Delta D_\sigma u \tag{21}$$

Thus, the new error equation becomes

$$\dot{e} = (A_\sigma - L_\sigma C_\sigma)e + L_\sigma e_y = (A_\sigma - L_\sigma C_\sigma)e + L_\sigma \Delta D_\sigma u \tag{22}$$

At this point, the error term $\Delta D_\sigma u$ is introduced as a new disturbance term into the observer system. This disturbance term will affect the convergence of the error dynamics and may lead to observer increased error.

However, the ESR of a supercapacitor is generally very small. Even though it may increase after prolonged use, the absolute change remains minimal, with the value of ΔD_σ typically in the order of 10^{-4} or lower. Therefore, the value of the error term $L_\sigma \Delta D_\sigma u$ is relatively small, making it still reliable to use this observer for supercapacitors.

4. Experimental Validation

This section will focus on the experiments. We will first introduce the hardware platform and experimental parameters used, then evaluate the proposed observer under four different scenarios. Finally, we will summarize and discuss the conclusions drawn from each experiment.

4.1. Structure of Hardware Platform

The hardware setup is illustrated in Figure 5 and consists of the following key components: a control board, three supercapacitors, voltage and current data acquisition units, and a 12 V DC power source.

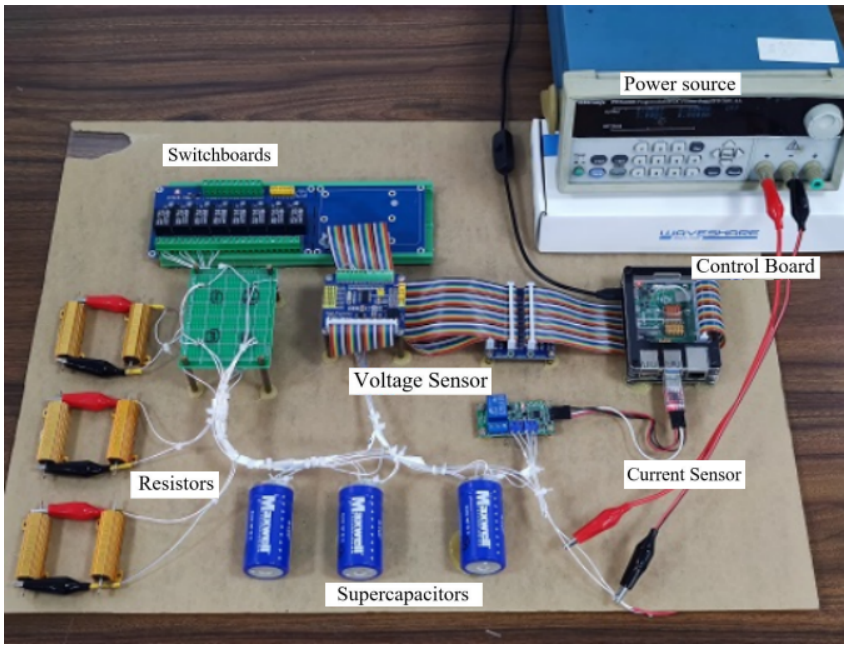

Figure 5. Hardware platform used for experimental validation.

Control Board: The platform's controller is a Raspberry Pi 4B with 8GB RAM running Raspberry Pi OS, featuring GPIO output, SPI communication, and serial communication.

Supercapacitors: Three Maxwell BCAP0310 supercapacitors (Yongin-si, Republic of Korea) are connected in series, balanced using RPi Relay Board (B) relay modules and RX24-50W equalizing resistors.

Voltage Sensor: A high-precision AD/DA board, equipped with an ADS1256 chip, provides 8 channels of 24-bit ADC (4 differential) at a maximum sampling rate of 30 ksps, along with a DAC8532 chip for 2 channels of a 16-bit DAC.

Current Sensor: An INA238 Current Sensor, with a 2 mΩ sampling resistance, detects currents up to 30 A with 0.05% accuracy, communicating data via serial communication.

Power Source: The Tektronix PWS4305 power supply (Beaverton, OR, USA), known for its 0.03% voltage accuracy and 0.05% current accuracy, provides charging current for the supercapacitors, while an external 12 V DC power supply powers the control board and sensors.

The operation process of the platform is as follows: The Raspberry Pi 4B runs the control program for the entire balancing and charging process. During charging, the controller uses SPI to monitor the voltage of each supercapacitor via the AD/DA Board. When a cell's voltage exceeds the set threshold, the controller activates the corresponding relay on the RPi Relay Board (B) via GPIO for balancing protection. The INA238 Current Sensor measures the charging current for further analysis.

4.2. Experimental Parameters

(1) Physical Parameters: According to Maxwell's specifications, the BCAP0310 supercapacitor has a rated capacitance of 310 F and a rated voltage of 2.70 V, with an absolute maximum voltage of 2.85 V. It operates between −40 °C and 65 °C, with our tests conducted at 25 °C, where the estimated DC life is 10 years, after which capacitance may decrease by up to 20% and ESR may increase by up to 100%.

To measure the capacitance and ESR, we followed the specified test current and waveform. With a maximum charging current of 10A, the measurements yielded the following results: for the first supercapacitor, C_{eq} = 298.455 F, r = 2.031 mΩ, and v_{rated} = 2.693 V; for the second, C_{eq} = 315.285 F, r = 1.967 mΩ, and v_{rated} = 2.608 V; and for the third, C_{eq} = 330.037 F, r = 1.978 mΩ, and v_{rated} = 2.769 V.

(2) System Parameters: For our experiments, we set the observer gain L to 0.2, a value determined to be suitable based on our theoretical analysis (Lemma 2) and confirmed through experimental observations.The charging current(i) is always set to 2 A.

4.3. Experimental Results

We designed three distinct experiments to compare the performance of our proposed observer against other observer implementations.

(1) Case 1: In this case, we focus on evaluating the robustness of our proposed observer (Equation (19)) against parameter uncertainties, comparing it to a standard open-loop observer (Equation (12)). To simulate a realistic scenario where component parameters may deviate from their nominal values, we introduced deviations of 10% and 20% in the capacitance value within the system parameters.

For this experiment, we charge the system using a constant current (CC) source at 2 A, with all three switches deactivated. Our focus is on the first supercapacitor cell, initialized at a voltage of 0.1 V, corresponding to an initial SOC of approximately 3.67%. The proposed observer and open-loop observer are both initialized at 15% SOC. We switched the switch to start charging the supercapacitor at t = 8 s and stopped charging again at at t = 124 s.

Figure 6 presents the experimental results. As evident from the plots, while the proposed observer exhibits an initial lag behind the true SOC, it rapidly converges and maintains its tracking error within 1% within approximately 5 s. In contrast, the open-loop observer struggles to achieve accurate tracking, as shown in Figure 6a, where a persistent error is observed with a 10% capacitance deviation. In Figure 6b, when the parameter deviation reaches 20%, the error worsens further. Table 2 contains SOC data at the end of charging. This highlights the superior robustness of our proposed observer in the presence of real-world parameter uncertainties.

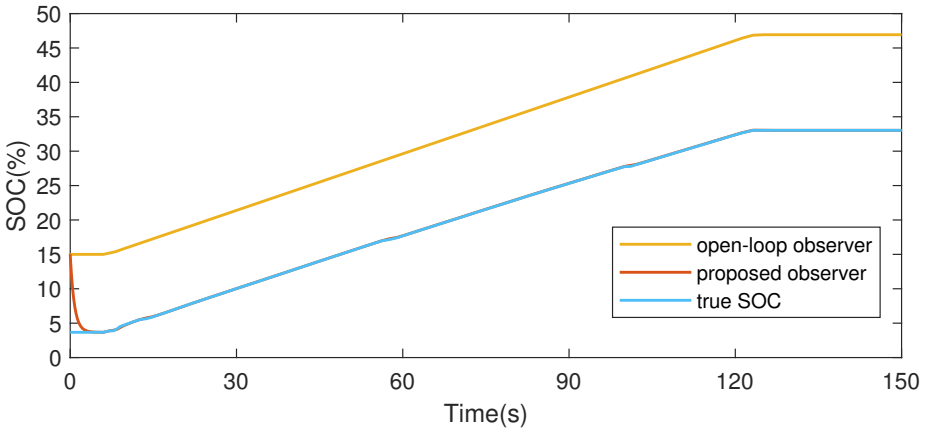

(a)

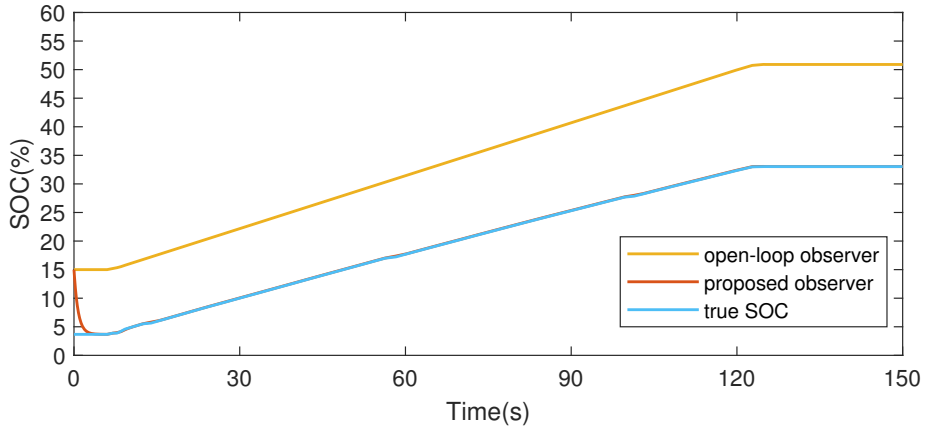

(b)

Figure 6. *Cont.*

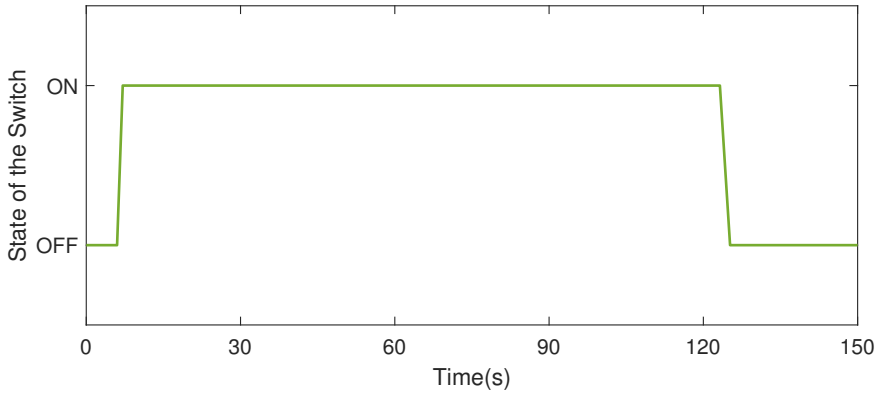

(**c**)

Figure 6. Comparison between the proposed observer and the open-loop observer. (**a**) SOC estimation with 10% capacitance variations. (**b**) SOC estimation with 20% capacitance variations. (**c**) Changes in the switch.

Table 2. SOC (%) at the end of charging in case 1.

	10% Capacitance Variations	20% Capacitance Variations
True Value	33.02	33.07
Proposed Observer	33.02	33.11
Open-loop Observer	46.92	50.95

(2) Case 2: In this experiment, we evaluated the observers' ability to adapt to changing operating conditions and accurately estimate the SOC during dynamic charging scenarios. As depicted in Figure 7b, to achieve this, we still used the first supercapacitor and switched the circuit again one minute after stopping the charging in case 1, at t = 184 s, and continued charging until t = 270 s. A capacitance deviation of 10% was maintained, while the initial voltage and observer states remained consistent with the previous experiment.

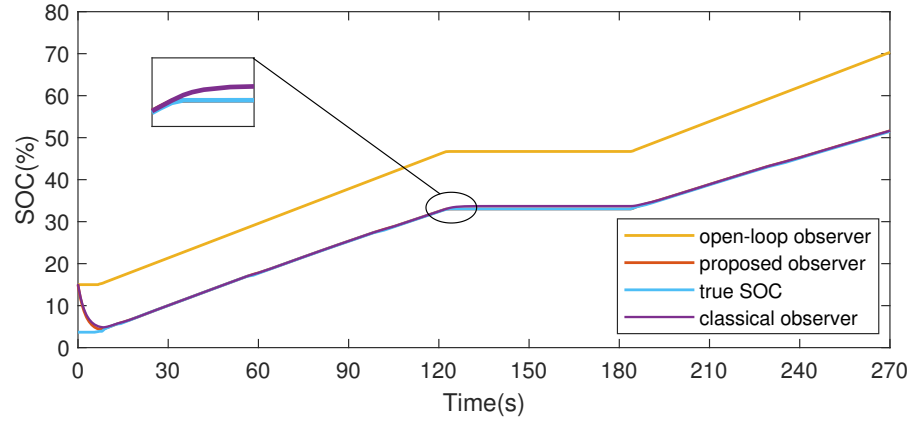

(**a**)

Figure 7. *Cont.*

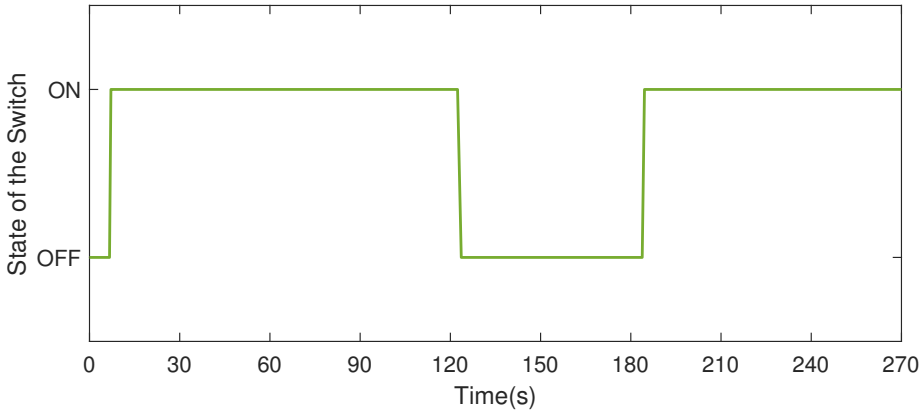

(**b**)

Figure 7. Comparison of SOC estimation performance during dynamic charging with capacitance variations. (**a**) SOC estimation with 10% capacitance variations. (**b**) Changes in the switch.

The classical non-switching Luenberger observer, defined in Equation (23), was incorporated into this evaluation, alongside the open-loop and proposed closed-loop observers.

$$\begin{cases} \dot{\text{SOC}} = A_1\text{SOC} + B_1 i + L_1(v - \hat{v}) \\ \hat{v} = C_1\hat{\text{SOC}} + \text{D}_1 i \end{cases} \tag{23}$$

As depicted in Figure 7a and Table 3, the proposed observer exhibited rapid convergence, achieving a tracking error of less than 1% by t = 7 s. This highlights its ability to quickly adapt to changing system dynamics.

Table 3. Comparison between the proposed observer, open-loop observer, and the classical observer.

	First Convergence Time (s)	Final SOC (%)	Maximum Absolute Error (%)
True Value	null	52.63	0
Proposed Observer	6.984	52.58	0.709
Classical Observer	10.527	52.89	3.602
Open-loop Observer	null	70.50	>50

The open-loop observer, as expected, continued to exhibit significant tracking errors throughout the experiment. The classical observer, while demonstrating improved performance compared to the open-loop approach, exhibited slower convergence initially and a noticeable error spike after the resumption of charging. This suggests that the non-switching nature of the classical observer limits its ability to effectively handle dynamic changes in the system.

In summary, this experiment demonstrates the superior performance of the proposed observer in handling dynamic charging scenarios and adapting to switching events, further emphasizing its suitability for real-world supercapacitor applications where operating conditions can vary significantly.

Since the proposed observer's estimation of the SOC remained very close to the actual SOC after the supercapacitor charging was completed in the next two experiments, the actual SOC values have been omitted from the subsequent tables.

(3) Case 3: This experiment investigates the observers' performance under a more complex scenario involving active balancing of the supercapacitor cells. We implemented the active balancing technique described in [19] to charge the second and third supercapacitors simultaneously.

The initial voltages of the second and third cells were set to 0.1 V and 0.9 V, respectively, while maintaining a constant charging current of 2 A. A 10% capacitance error was introduced to assess the observers' robustness. Both the proposed and classical observers were initialized at 15% SOC. We started charging at t = 8 s and stopped at t = 242 s.

Figure 8a shows the SOC of two supercapacitors. Due to the presence of the active balancing system, the third supercapacitor, which initially has a higher SOC, will wait until the SOC of the second supercapacitor matches its own before switching on to start charging, as illustrated in Figure 8b. It begins charging only after t = 125 s. Figure 9a,b, respectively, show the SOC estimation of the second and third supercapacitors.

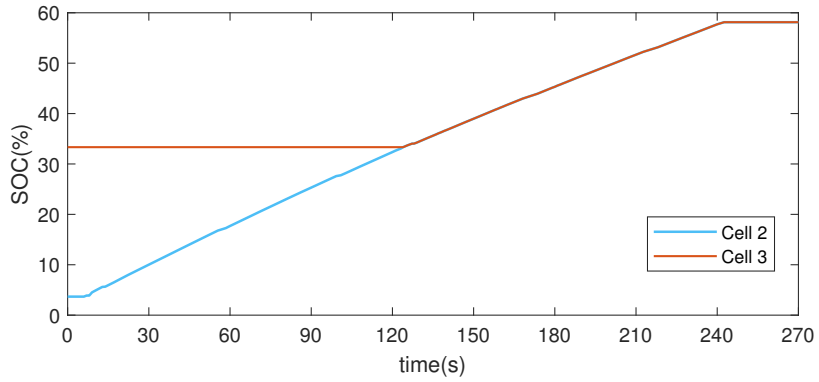

(**a**)

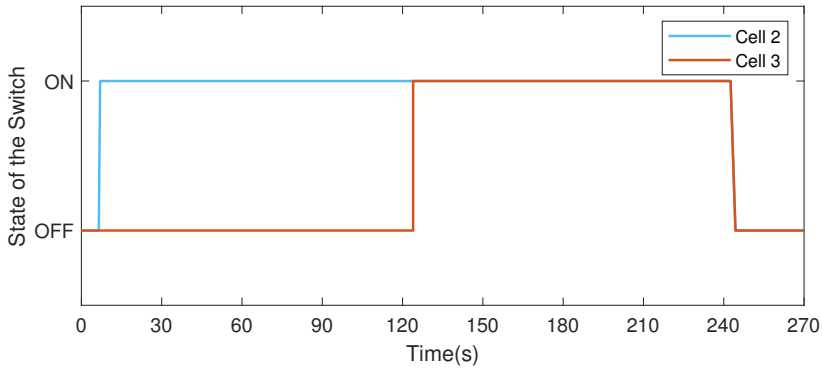

(**b**)

Figure 8. The charging process with active balancing strategy. (**a**) SOC evolution of the cells during active balancing. (**b**) Switching sequence during active balancing.

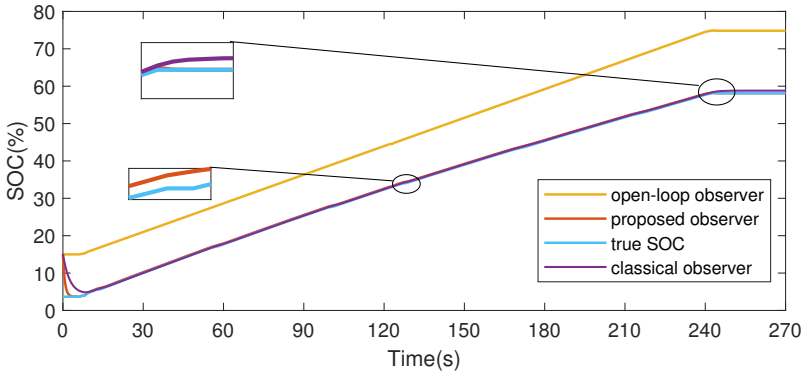

(**a**)

Figure 9. *Cont.*

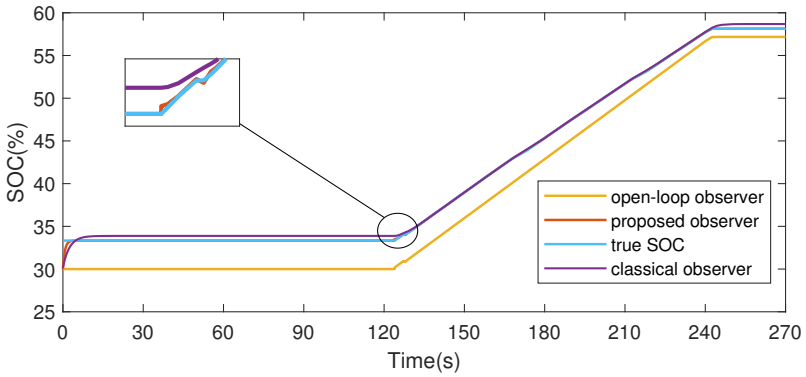

(**b**)

Figure 9. Comparison in active balancing charging process. (**a**) SOC estimation of the second supercapacitor. (**b**) SOC estimation of the third supercapacitor.

Focusing on the second supercapacitor, according to Tables 4 and 5, the proposed observer demonstrates a significantly superior performance, achieving a tracking error below 1% within 3 s. While the classical observer eventually approaches the true SOC, its convergence speed and accuracy lag behind the proposed observer, particularly after switching events. Specifically, after the switching moment, the classical observer's tracking error rises to 2.7%, whereas the proposed observer maintains an error below 0.5%.

Table 4. SOC estimation of the second cell.

	First Convergence Time (s)	Final SOC (%)	Maximum Absolute Error (%)
Open-loop Observer	null	74.84	>50
Classical Observer	8.446	58.81	2.735
Proposed Observer	2.821	58.13	0.433

Table 5. SOC estimation of the third cell.

	First Convergence Time (s)	Final SOC (%)	Maximum Absolute Error (%)
Open-loop Observer	null	57.17	10
Classical Observer	127.259	58.68	1.09
Proposed Observer	2.238	58.13	0.172

Similar trends are observed for the third supercapacitor, with the proposed observer exhibiting stable and accurate tracking performance despite the extended initial charging time, which negatively impacts the classical observer's performance.

In this experiment, the open-loop observer still performed poorly, failing to converge in estimating the SOC for both supercapacitors, highlighting its inadequacy in complex scenarios.

These findings underscore the robustness and accuracy of the proposed switching observer in handling the complexities of active balancing, further solidifying its suitability for demanding supercapacitor applications.

(4) Case 4: In this case, we introduce the Kalman Filter, a widely used tool for state estimation, to estimate the State of Charge (SOC) of the supercapacitor. We employ the same switching scheme as in case 1 and also consider a 10% parameter deviation. However, unlike before, we separately consider the cases where the capacitance C_{eq} and ESR in the RC model have fluctuations.

As shown in the Figure 10, in both experiments, the open-loop observer's error is unacceptable, while both the Kalman Filter and the proposed observer exhibit stable performance. Although both converge to the actual SOC when charging stops, there are still some performance differences.

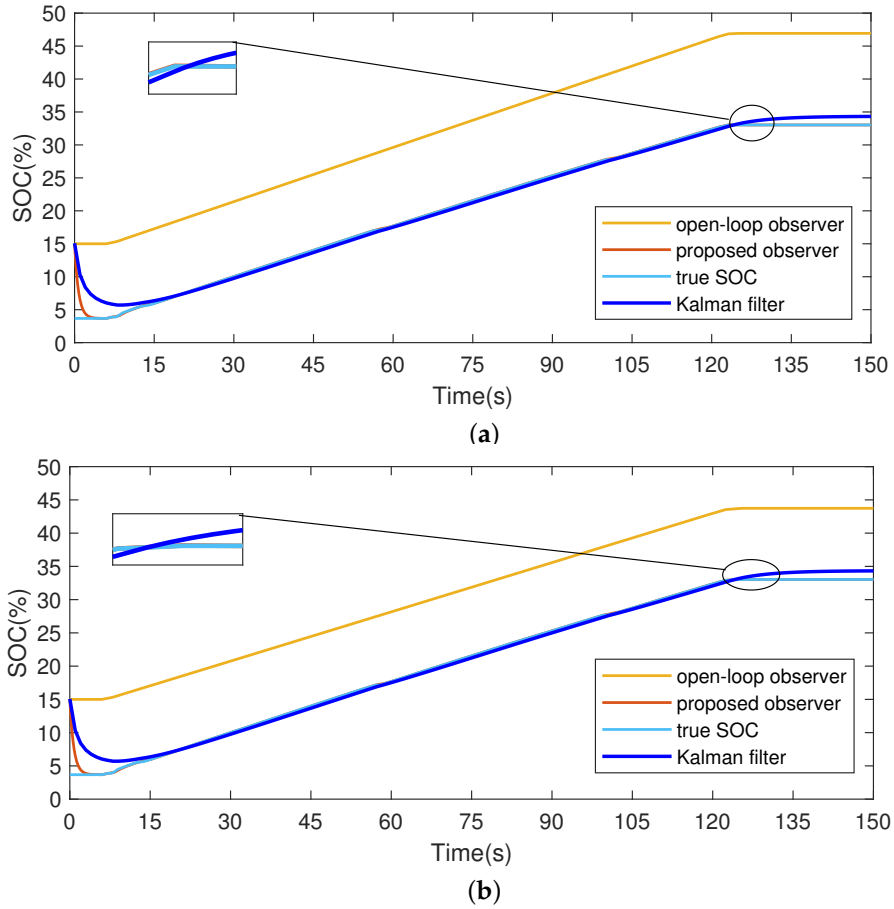

Figure 10. Comparison with Kalman Filter. (**a**) SOC estimation with 10% capacitance variations. (**b**) SOC estimation with 10% ESR variations.

According to Tables 6 and 7, during the period from 0 to 5 s when the supercapacitor is not charging, the SOC of the proposed observer quickly converges to the true value, while the Kalman Filter only approaches the true value after next 10 s of charging. However, after this period, the Kalman Filter still exhibits larger errors. Although these errors decrease over time as charging progresses, they do not fully converge even by the time charging stops.

Table 6. Comparison of the proposed observer and Kalman Filter with 10% capacitance variations.

	First Convergence Time (s)	Maximum Absolute Error (%)
Proposed Observer	2.639	<0.3
Open-loop Observer	null	>50

Table 7. Comparison of the proposed observer and Kalman Filter with 10% ESR variations.

	First Convergence Time (s)	Maximum Absolute Error (%)
Proposed Observer	2.631	<0.3
Kalman Filter	14.937	4.140
Open-loop Observer	null	>50

Furthermore, this experiment considers the impact of ESR variation on SOC estimation. Since the supercapacitor used in the experiment has a relatively small ESR, its parameter fluctuation has a relatively small impact on SOC estimation, similar to the same proportional change in capacitance. However, further discussion is needed for supercapacitors that have been used for a long time and have experienced significant ESR increases.

4.4. Discussion

Faster Convergence and Accurate Tracking: The proposed observer exhibits the fastest convergence rate, even when initial state errors are present. It maintains accurate SOC tracking throughout the charging process, effectively handling switching events without significant deviations. This is crucial for real-time applications where continuous and accurate SOC estimation is essential.

Robustness to Parameter Variations: A key advantage of the proposed observer lies in its robustness to parameter uncertainties. Even with capacitance errors as high as 10% or 20%, the observer consistently converges to the true SOC value. This robustness is particularly valuable in practical applications where accurately measuring and maintaining precise supercapacitor parameters can be challenging due to aging and operating conditions.

Addressing Limitations of Existing Methods: The experiments highlight the limitations of both classical and open-loop observers. Classical observers, while able to converge eventually, suffer from slower convergence speeds and significant deviations in SOC estimation after charging interruptions. This inability to maintain accuracy during dynamic operation restricts their applicability. Open-loop observers, on the other hand, exhibit poor convergence and high sensitivity to both initial state errors and parameter variations, rendering them unsuitable for reliable SOC estimation.

5. Conclusions

This paper addressed the challenge of accurate State-of-Charge (SOC) estimation for supercapacitors in reconfigurable circuits, a critical aspect for ensuring reliable operation and efficient energy management in these systems. We began by establishing a comprehensive mathematical model encompassing the two distinct operating states of supercapacitors within reconfigurable circuits. This model was rigorously analyzed to demonstrate its continuity and observability properties, laying the foundation for observer design.

Recognizing the limitations of traditional observers in handling the dynamic nature of reconfigurable circuits, we proposed a novel switching observer tailored to this specific application. To rigorously evaluate its performance, we conducted a series of experiments on a hardware platform, comparing its performance against both classical and open-loop observers. The experimental results unequivocally demonstrated the superiority of the proposed switching observer, showcasing its faster convergence speed, enhanced robustness to parameter variations, and accurate tracking capabilities even during dynamic charging and switching events.

Future research directions include the following:

(1) Combining the switching observer framework with more sophisticated estimation algorithms, such as switching Kalman Filtering or sliding-mode observers, could further enhance its convergence speed and disturbance rejection capabilities. This integration could lead to even more accurate and robust SOC estimation, particularly in noisy environments or under rapidly changing operating conditions.

(2) The current supercapacitor model, while effective, could be further refined by incorporating temperature dependencies and variations in ESR. These factors can significantly influence supercapacitor behavior, and their inclusion in the model would enhance the observer's accuracy, particularly over a wider range of operating temperatures and during long-term operation. This could involve developing more sophisticated temperature and aging models for the supercapacitor parameters, potentially leveraging data-driven approaches for enhanced accuracy.

Author Contributions: Methodology, H.L. and Z.Z.; data curation, Z.Z.; writing—original draft preparation, H.L. and Z.Z.; writing—review and editing, C.H. All authors have read and agreed to the published version of the manuscript.

Funding: This research was sponsored in part by the National Natural Science Foundation of China (No. 62177046 and 62477046), Hunan 14th Five-Year Plan Educational Science Research Project(No. XJK23AJD022 and XJK23AJD021), Hunan Social Science Foundation (No. 22YBA012), and High Performance Computing Center of Central South University.

Institutional Review Board Statement: Not applicable.

Informed Consent Statement: Not applicable.

Data Availability Statement: The data presented in this study are available on request from the corresponding author. The data are not publicly available due to privacy and personal reasons.

Conflicts of Interest: The authors declare no conflicts of interest.

Abbreviations

The following abbreviations are used in this manuscript:

SOC	State of Charge
ESR	Equivalent series resistance

References

1. Şahin, M.E.; Blaabjerg, F.; Sangwongwanich, A. A Comprehensive Review on Supercapacitor Applications and Developments. *Energies* **2022**, *15*, 674. [CrossRef]
2. Molahalli, V.; Chaithrashree, K.; Singh, M.K.; Agrawal, M.; Krishnan, S.G.; Hegde, G. Past Decade of Supercapacitor Research–Lessons Learned for Future Innovations. *J. Energy Storage* **2023**, *70*, 108062. [CrossRef]
3. Ceraolo, M.; Lutzemberger, G.; Poli, D. State-of-charge evaluation of supercapacitors. *J. Energy Storage* **2017**, *11*, 211–218. [CrossRef]
4. Pipicelli, M.; Sessa, B.; De Nola, F.; Gimelli, A.; Di Blasio, G. Assessment of Battery–Supercapacitor Topologies of an Electric Vehicle under Real Driving Conditions. *Vehicles* **2023**, *5*, 424–445. [CrossRef]
5. Liu, C.; Li, Q.; Wang, K. State-of-charge Estimation and Remaining Useful Life Prediction of Supercapacitors. *Renew. Sustain. Energy Rev.* **2021**, *150*, 111408. [CrossRef]
6. Ch, ran, V.; Patil, C.K.; Karthick, A.; Ganeshaperumal, D.; Rahim, R.; Ghosh, A. State of Charge Estimation of Lithium-ion Battery for Electric Vehicles Using Machine Learning Algorithms. *World Electr. Veh. J.* **2021**, *12*, 38. [CrossRef]
7. Chemali, E.; Kollmeyer, P.J.; Preindl, M.; Emadi, A. State-of-charge estimation of Li-ion batteries using deep neural networks: A machine learning approach. *J. Power Sources* **2018**, *400*, 242–255. [CrossRef]
8. Zahid, T.; Xu, K.; Li, W.; Li, C.; Li, H. State of Charge Estimation for Electric Vehicle Power Battery Using Advanced Machine Learning Algorithm Under Diversified Drive Cycles. *Energy* **2018**, *162*, 871–882. [CrossRef]
9. Yang, F.; Zhang, S.; Li, W.; Miao, Q. State-of-charge Estimation of Lithium-ion Batteries Using LSTM and UKF. *Energy* **2020**, *201*, 117664. [CrossRef]
10. Fornaro, P.; Puleston, P.; Battaiotto, P. On-line Parameter Estimation of a Lithium-Ion Battery/Supercapacitor Storage System Using Filtering Sliding Mode Differentiators. *J. Energy Storage* **2020**, *32*, 101889. [CrossRef]
11. El Fadil, H.; Belhaj, F.; Rachid, A.; Giri, F.; Ahmed-Ali, T. Nonlinear Modeling and Observer for Supercapacitors in Electric Vehicle Applications. *IFAC-PapersOnLine* **2017**, *50*, 1898–1903. [CrossRef]
12. Zhou, Y., Huang, Z., Peng, J., Li, H. and Liao, H. A Generalized Extended State Observer for Supercapacitor State of Charge Estimation Under Disturbances. In Proceedings of the 2017 American Control Conference (ACC), Seattle, WA, USA, 24–26 May 2017; IEEE: Piscataway, NJ, USA, 2017; pp. 4029–4034.
13. Ren, J.; Xu, Y.; Zhang, H.; Yang, F.; Yang, Y.; Wang, X.; Jin, P.; Huang, D. State of Charge Estimation of Ultracapacitor Based on Forgetting Factor Recursive Least Square and Extended Kalman Filter Algorithm at Full Temperature Range. *Heliyon* **2022**, *8*, 11146. [CrossRef] [PubMed]
14. Yang, H.; Sun, X.; An, Y.; Zhang, X.; Wei, T.; Ma, Y. Online Parameters Identification and State of Charge Estimation for Lithium-Ion Capacitor Based on Improved Cubature Kalman Filter. *J. Energy Storage* **2019**, *24*, 100810. [CrossRef]
15. Xu, Y.; Zhang, H.; Yang, F.; Tong, L.; Yan, D.; Yang, Y.; Ren, J.; Ma, L.; Wang, Y. State of Charge Estimation of Supercapacitors Based on Multi-Innovation Unscented Kalman Filter under a Wide Temperature Range. *Int. J. Energy Res.* **2022**, *46*, 16716–16735. [CrossRef]
16. Zhang, J.; Xiao, B.; Niu, G.; Xie, X.; Wu, S. Joint Estimation of State-of-charge and State-of-power for Hybrid Supercapacitors Using Fractional-order Adaptive Unscented Kalman Filter. *Energy* **2024**, *294*, 130942. [CrossRef]
17. Linzen, D.; Buller, S.; Karden, E.; De Doncker, R.W. Analysis and evaluation of charge-balancing circuits on performance, reliability, and lifetime of supercapacitor systems. *IEEE Trans. Ind. Appl.* **2005**, *41*, 1135–1141. [CrossRef]

18. Li, H.; Peng, J.; He, J.; Huang, Z.; Wang, J.; He, L.; Pan, J. Pinning-Based Switching Control of Cyber-Physical Supercapacitor Energy Storage Systems. *IEEE Trans. Control. Syst. Technol.* **2019**, *28*, 1520–1533. [CrossRef]
19. Li, H.; He, W.; Fang, X.; Li, S. State-of-Charge Estimation of Supercapacitors: A Switched Systems Approach. *IEEE Trans. Transp. Electrif.* **2023**, *early access*. [CrossRef]
20. Jiang, F.; Meng, Z.; Li, H.; Liao, H.; Jiao, Y.; Han, M.; Peng, J.; Huang, Z. Consensus-based cell balancing of reconfigurable supercapacitors. *IEEE Trans. Ind. Appl.* **2020**, *56*, 4146–4154. [CrossRef]